The Global Stationary Wave Response to Climate Change in a Coupled GCM

RENU JOSEPH AND MINGFANG TING*

Department of Atmospheric Sciences, University of Illinois at Urbana–Champaign, Urbana, Illinois

PAUL J. KUSHNER

NOAA/GFDL, Princeton, New Jersey

(Manuscript received 24 March 2003, in final form 1 August 2003)

ABSTRACT

The stationary wave response to global climate change in the Geophysical Fluid Dynamics Laboratory's R30 coupled ocean–atmosphere GCM is studied. An ensemble of climate change simulations that use a standard prescription for time-dependent increases of greenhouse gas and sulfate aerosol concentrations is compared to a multiple-century control simulation with these constituents fixed at preindustrial levels. The primary response to climate change is to zonalize the atmospheric circulation, that is, to reduce the amplitude of the stationary waves in all seasons. This zonalization is particularly strong in the boreal summer over the Tropics. In January, changes in the stationary waves resemble that of an El Niño, and all months exhibit an El Niño–like increase of precipitation in the central tropical Pacific.

The dynamics of the stationary wave changes are studied with a linear stationary wave model, which is shown to simulate the stationary wave response to climate change remarkably well. The linear model is used to decompose the response into parts associated with changes to the zonal-mean basic state and with changes to the zonally asymmetric ''forcings'' such as diabatic heating and transient eddy fluxes. The decomposition reveals that at least as much of the climate change response is accounted for by the change to the zonal-mean basic state as by the change to the zonally asymmetric forcings. For the January response in the Pacific–North American sector, it is also found that the diabatic heating forcing contribution dominates the climate change response but is significantly cancelled and phase shifted by the transient eddy forcing. The importance of the zonal mean and of the diabatic heating forcing contrasts strongly with previous linear stationary wave models of the El Niño, despite the similarity of the January stationary wave response to El Niño. In particular, in El Niño, changes to the zonal-mean circulation contribute little to the stationary wave response, and the transient eddy forcing dominates. The conclusions from the linear stationary wave model apparently contradict previous findings on the stationary wave response to climate change response in a coarse-resolution version of this model.

1. Introduction

Public interest in the environmental and societal impacts of increased atmospheric greenhouse gas concentrations has increased substantially in the past two decades. There have been numerous studies addressing the issue of climate change in coupled ocean–atmosphere models with increasing greenhouse gas and sulfate aerosol concentrations (e.g., Meehl et al. 2000a,b; Mitchell and Johns 1997). Although many of these studies have described the global and regional aspects of climate change, they have placed less emphasis upon explaining the dynamics of the climate change response of the atmospheric circulation.

Atmospheric stationary waves, defined as departures from the climatological- and zonal-mean state, are closely linked to regional climate and therefore play a key role in regional climate change. For example, a region downstream of the stationary troughs, such as East Asia or the eastern United States, is usually cloudier and has more annual rainfall than a region controlled by a stationary ridge, such as the southwestern United States. If stationary waves control regional climate, changes to the stationary waves brought about by greenhouse warming could be linked to significant regional climate change. Thus, the potential for stationary waves to be altered by climate change is linked to regional climate change issues of societal importance. From a broader perspective, to better understand the causes of regional climate anomalies, it is important to first understand the stationary wave dynamical mechanisms responsible for those anomalies.

* Current affiliation: Lamont-Doherty Earth Observatory, Columbia University, Palisades, New York.

Corresponding author address: Dr. Renu Joseph, Department of Meteorology, University of Maryland, College Park, 3420 Computer and Space Sciences Building, College Park, MD 20742.
E-mail: rjoseph@atmos.umd.edu

The goal of this study is to elucidate the stationary wave response and the mechanisms underlying this response when the climate system is perturbed by anthropogenic climate change. We use the coupled ocean–atmosphere general circulation model (GCM) developed by the Geophysical Fluid Dynamics Laboratory (GFDL) climate dynamics group in the 1980s and 1990s, also known as the GFDL R30 GCM. We examine the response of this model's simulated stationary wave patterns to a standard scenario of greenhouse warming. Among other goals, we wish to explore the full seasonal cycle of this response and to explore the robustness of this response within an ensemble of integrations.

There has been relatively little work on the stationary wave response to climate change. Stephenson and Held (1993), among the first of such studies, find a Pacific–North American (PNA) regional response in the R15 version of the GFDL GCM with a high over the eastern Pacific and eastern Canada and a low over the western United States. The response is consistent with the anomalous circulation of an El Niño event. Stephenson and Held find that the dynamics of the boreal-winter stationary wave response is very similar to that of an El Niño. Due to the low resolution of their model and its consequent poor simulation of transient eddy dynamics, they caution that results for high-resolution models might differ. Recent studies (Goswami 1998; Ting et al. 2001) have shown that the GFDL R30 atmospheric model can simulate the stationary waves and the Asian monsoon circulation well compared to the R15 model. It is thus useful, at this point, to reexamine the stationary wave response to climate change and to compare this response to the Stephenson and Held (1993) study. We extend the Stephenson and Held study by examining seasons other than the boreal winter. The summer stationary wave response to climate change, and its impact upon, for example, the agricultural growing season, is of particular societal importance.

An important advantage of approaching regional climate change from a stationary wave perspective is that stationary wave dynamics is amenable to linear theory and to linear modeling approaches. Many previous studies (e.g., Nigam et al. 1986, 1988; Chen and Trenberth 1988a,b; Valdes and Hoskins 1989; Wang and Ting 1999) have shown that linear models have been successful in analyzing the dynamics of planetary stationary waves. Linear models have also been used to study stationary wave anomalies, such as those due to natural variability (Branstator 1992; Ting and Lau 1993; Ting et al. 1996), ENSO-induced anomalies (Held et al. 1989; Ting and Hoerling 1993; Hoerling and Ting 1994), and circulation anomalies associated with droughts and floods (Liu et al. 1998). Here, we use a baroclinic stationary wave model linearized about a zonally symmetric flow to analyze the stationary wave response to greenhouse warming simulated in the coupled model.

We are particularly interested in the relationship between the stationary wave response and the circulation anomalies associated with an El Niño. Besides Stephenson and Held (1993), many other studies have also indicated an El Niño–like response to climate change (e.g., Knutson and Manabe 1995, 1998; Meehl and Washington 1996; Meehl et. al. 2000a,b; Cai and Whetton 2001). However, the linear model will show that a climate change response that resembles the El Niño in, for example, its precipitation field, is not necessarily dynamically similar to an El Niño. This highlights the importance of carefully studying and comparing the dynamical mechanisms of the circulation response to climate change for various models.

The coupled model and the linear model are described in section 2. The coupled model's climate change response is presented in section 3, with a focus on the stationary wave response. A comparison of the control simulation and observations is done in this section to evaluate the realism of the GFDL simulation. Section 4 presents the results of our linear-model diagnosis. Finally, a summary and conclusions are provided in section 5.

2. Methodology

a. Climate change experiments

The GFDL R30 coupled GCM consists of the GFDL R30 atmospheric GCM with 14 sigma levels and the Modular Ocean Model (MOM1) with approximately 2° resolution in latitude and longitude, as documented in Delworth et al. (2002). The control simulation is a 1000-yr-long integration with greenhouse gas and sulfate aerosol concentrations fixed at preindustrial levels. The perturbation to this control consists of an ensemble of three Intergovernmental Panel on Climate Change (IPCC) ''IS92a scenario'' simulations (Mitchell et al. 1995; Haywood et al. 1997) in which the greenhouse gas and sulfate aerosol concentrations are gradually increased. The three climate change scenario integrations are 225 yr long and branch off the control at years 116, 351, and 401. Using the Delworth et al. (2002) nomenclature, the control simulation we examine here is CONTROL_B, and the scenario simulations are GS_B_1, GS_B_2, and GS_B_3. The comparison between the three scenario runs provides a statistical significance check of the climate change signal. The climate change response is defined as the difference, from the climatological mean of the last 800 yr of the control integrations, of the climatological mean of the last 25 yr of the scenario integrations. These last 25 yr correspond to the projection for the period from 2065 to 2089.

b. Linear stationary wave model

We use a much simpler, dry, linear, baroclinic, steady-state stationary wave model of the atmosphere to analyze the coupled model's response. This model solves the linear perturbation problem of the steady, zonally

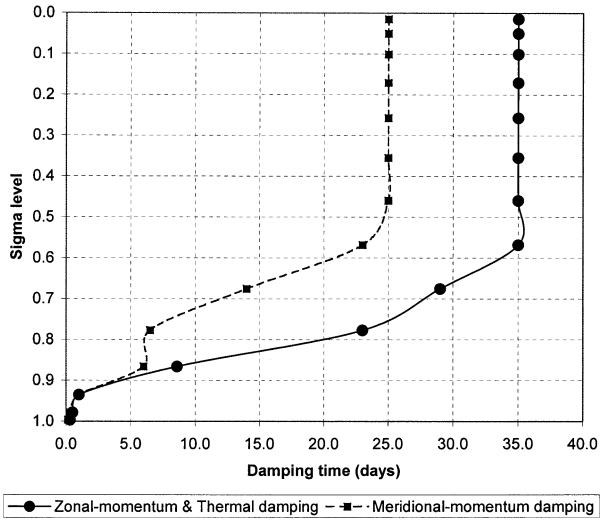

FIG. 1. Damping time scales as a function of model level for the Rayleigh friction coefficient in the zonal-momentum equation and the Newtonian damping coefficient in the thermodynamic equation (solid line). Damping time scale for the meridional momentum equation (dashed line).

asymmetric circulation response to the zonally asymmetric forcings superimposed on a steady, zonal-mean basic flow. The linear model is that of Ting et al. (2001) (see also Ting 1994 and Wang and Ting 1999); its grid matches the R30 coupled model's grid in the horizontal and vertical. The model equations are the prognostic equations for vorticity, divergence, temperature, and log of surface pressure, in which the time tendencies have been set to zero, plus diagnostic equations describing mass continuity and hydrostatic balance.

To eliminate small-scale noise in the solution, biharmonic diffusion with a global coefficient equal to 10^{17} $m^4\ s^{-1}$ is applied to the vorticity, divergence, and temperature equations. In addition, Rayleigh drag is applied to the momentum tendency via the vorticity and divergence equations, and Newtonian cooling is applied to the thermodynamic equation. The Rayleigh friction and Newtonian cooling coefficients in the 14 model layers are shown in Fig. 1. Notice that the time scale of the damping decreases and, hence, the strength of the damping increases closer to the surface; this is to mimic the turbulent vertical momentum and heat transfers in the planetary boundary layer. The coefficients in Fig. 1 are estimates based on the GFDL GCM obtained from regressing the vertical diffusion of momentum against the horizontal velocity as in Ting et al. (2001).

Expressed schematically, the linear model solves the steady-state problem

$$\psi^* = L_{\overline{\psi}}(f), \tag{1}$$

where ψ^* is the linear model's stationary wave solution, $\overline{\psi}$ is the basic state from the coupled model, f is the zonally asymmetric forcing from the coupled model, and L is an operator representing the stationary wave dynamics. The basic state from the coupled model, $\overline{\psi}$, includes the climatological monthly mean of the zonal-mean horizontal wind, temperature, and log of surface pressure. The zonally asymmetric forcing from the coupled model, f, includes orographic uplifting; diabatic heating; transient eddy vorticity, divergence, and heat flux convergences; and the so-called stationary nonlinearity. The latter consists of terms that have been neglected during linearization of the stationary wave heat, vorticity, and divergence flux terms and can be regarded as the representation of the GCM's stationary wave–wave (nonlinear) interactions. The orography and diabatic heating forcings are obtained directly from the GCM; the transient and stationary nonlinearity forcings have been derived from the monthly mean GCM data as in Ting (1994). The transient forcing is calculated as residuals in the vorticity, divergence, and thermodynamic equations using the monthly mean GCM outputs. Given that all terms in the GCM equations are known from the GCM outputs (including all advection terms, diabatic heating, and boundary momentum fluxes), this way of deriving the transients should not introduce any errors in the transient forcing except computer round-off errors.

Assume that $\overline{\psi}$ and f are the coupled-model control simulation's inputs so that ψ^* is the linear stationary wave solution for the control simulation. Let us then denote by $\{\delta\overline{\psi}, \delta f\}$ the climate change response of the zonal mean and the forcings, which are taken from the coupled-model climate change simulation. We denote the linear stationary wave model's climate change response as $\delta\psi^*$; it satisfies

$$\psi^* + \delta\psi^* = L_{\overline{\psi}+\delta\overline{\psi}}(f + \delta f). \tag{2}$$

Thus, from (1)–(2)

$$\begin{aligned}\delta\psi^* &= L_{\overline{\psi}+\delta\overline{\psi}}(\delta f) + L_{\overline{\psi}+\delta\overline{\psi}}(f) - L_{\overline{\psi}}(f)\\ &= \delta\psi_f^* + \delta\psi_b^*,\end{aligned} \tag{3}$$

where we define

$$\delta\psi_f^* = L_{\overline{\psi}+\delta\overline{\psi}}(\delta f) \approx L_{\overline{\psi}}(\delta f) \quad \text{and} \tag{4}$$

$$\delta\psi_b^* = L_{\overline{\psi}+\delta\overline{\psi}}(f) - L_{\overline{\psi}}(f). \tag{5}$$

From (4) and (5), we see that $\delta\psi_f^*$ represents to first order in perturbation amplitude, the part of the response associated with the change in forcing for a fixed basic state and $\delta\psi_b^*$ represents the part of the response associated with the change in the basic state for a fixed forcing.

Besides the decomposition (3)–(5), we will also consider a decomposition in which the response contributions from each of the four forcing terms in f are separated. Schematically, we write

$$f = \sum_{i=1}^{4} f_i \quad \text{and} \tag{6}$$

$$\delta\psi^* = \sum_{i=1}^{4} \delta\psi_i^*, \tag{7}$$

where

$$\delta\psi_i^* = L_{\overline{\psi}+\delta\overline{\psi}}(\delta f_i) + L_{\overline{\psi}+\delta\overline{\psi}}(f_i) - L_{\overline{\psi}}(f_i)$$
$$= \delta\psi_{f_i}^* + \delta\psi_{b_i}^*. \quad (8)$$

3. Stationary wave response to global warming in the coupled model

In this section, we describe the coupled model's stationary wave response to ''climate change,'' that is, to the increased greenhouse gas and sulfate aerosol concentrations. To represent the circulation response, we focus upon the upper-tropospheric (250 mb) and lower-tropospheric (850 mb) streamfunction fields. We also show the precipitation response, which is closely linked to the tropical-circulation and diabatic-heating responses. We present results for all four seasons with an emphasis on January and July.

We first evaluate the realism of the coupled GCM's simulated stationary wave field. We find that the coupled GCM well simulates the spatial pattern and amplitude of the climatological stationary waves, particularly when the stationary waves are the strongest. To show this, we present in Fig. 2a, the spatial pattern correlation, for the stationary wave streamfunction, between the control simulation and a 52-yr climatology from the National Centers for Environmental Prediction–National Center for Atmospheric Research (NCEP–NCAR) reanalysis. This quantity is shown as a function of climatological month and vertical level. The stationary wave spatial patterns has a correlation with the reanalysis that is greater than 0.7. The highest correlation is in the boreal summer season between 900 and 600 mb and in the upper troposphere between 150 and 300 mb. The correlation is the lowest in the transition seasons. To evaluate the strength of the simulated stationary waves, we compare in Figs. 2b and 2c the area-weighted global integral of the square of the stationary wave streamfunction amplitude for the reanalysis and the control simulation. The strength of the stationary wave field in the reanalysis shows a strong seasonal cycle in the upper troposphere and a less pronounced seasonal cycle in the lower troposphere. This seasonal cycle is well simulated in the control, although the simulation's field is slightly stronger.

We begin our examination of the stationary wave response to climate change by illustrating, in Fig. 3, the January stationary wave streamfunction response at 250 mb in each of the three ensemble realizations. The time periods involved in defining the response are described in section 2a. The similarity among Figs. 3a–c clearly indicates that the stationary wave response to climate change is statistically robust. Since we find that this robustness extends to other seasons and levels, we henceforth show only the ensemble-average response.

The ensemble-average streamfunction response at 250 mb for January, April, July, and October is shown in Fig. 4 along with the stationary waves of the control integration. In January, the change in upper-tropospheric

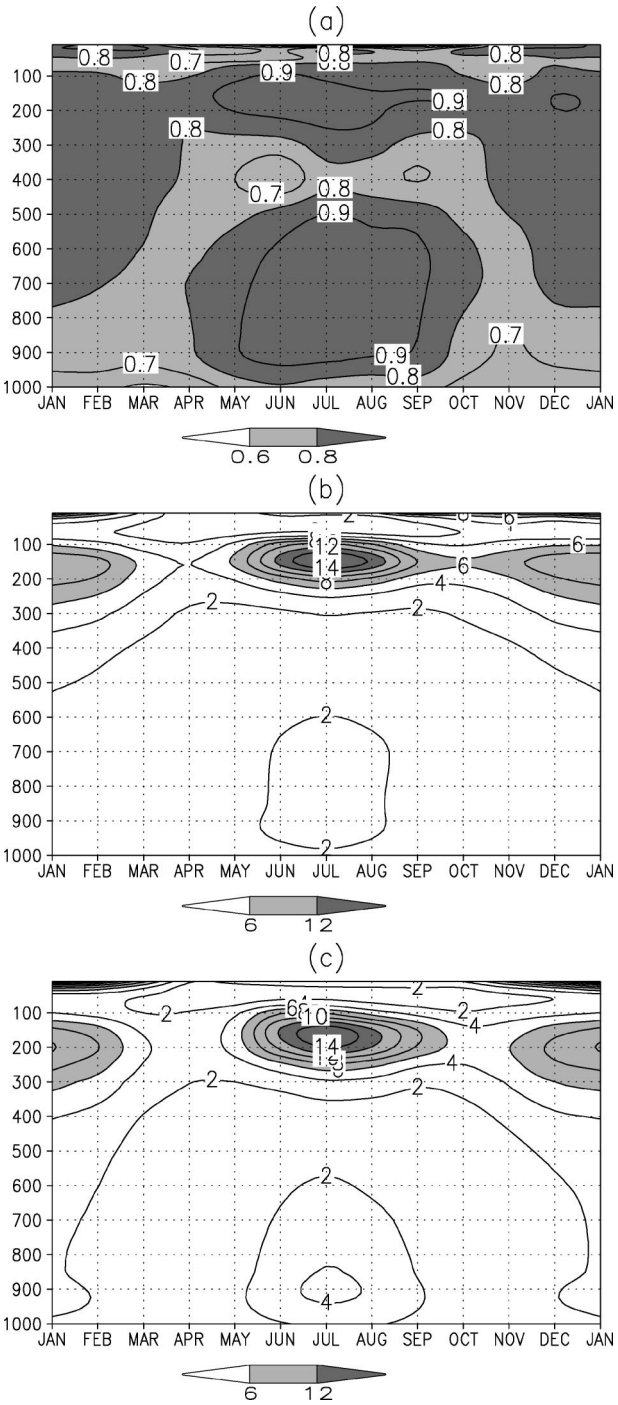

FIG. 2. (a) Area-weighted spatial pattern correlation between the 52-yr average of the NCEP–NCAR reanalysis and the control simulation's horizontal streamfunction as a function of pressure and climatological month. (b) Area-weighted global integral of the square of the stationary wave streamfunction amplitude for the NCEP–NCAR reanalysis. (c) As in (b) but for the control run of the coupled model. Contour interval is 10^{13} m^2 s^{-2}.

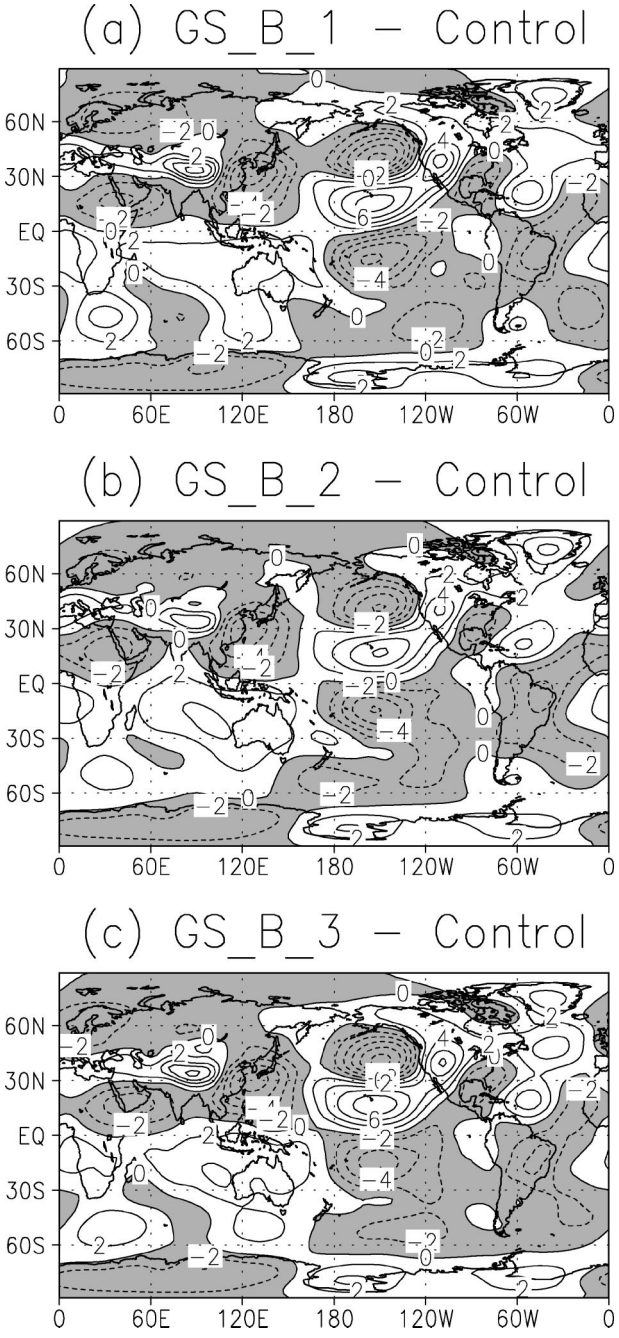

FIG. 3. Differences in stationary wave streamfunction at 250 mb between the climate change scenario integration and the control climate for the three climate change scenario ensemble members described in section 2a. Contour interval is 2×10^6 m^2 s^{-1} and negative values are shaded.

streamfunction in the Northern Hemisphere (NH) extratropics is manifested as an extension of the East Asian low into the Gulf of Alaska and as an intensified ridge from the western United States into northeast Canada and the North Atlantic. In the Tropics, the comparison between Figs. 4a and 4b indicates that the response is generally anticorrelated with the climatological stationary wave pattern for almost all of the features in both hemispheres. There is also an apparent eastward shift of the pattern in the central tropical Pacific. The anticorrelation in the Tropics implies that the stationary wave field responds to climate change by becoming weaker there.

The boreal winter stationary wave response in the NH extratropics resembles the atmospheric response to El Niño with a low centered over the Gulf of Alaska, a high over North America, and a low over the southeast United States. The pattern, however, differs significantly from the canonical El Niño pattern in that there is little indication of wave propagation from the Tropics to the mid and high latitudes. In this respect, the GFDL R30 response also differs from the GFDL R15 response to climate change (Stephenson and Held 1993), which is more wavelike and has a clearer tropical–extratropical connection. Later, we will point out other contrasts between the GFDL R15 and R30 models.

As stated in the introduction, we wish to examine the full seasonal cycle of the stationary wave response to climate change. In April, the stationary wave response is rather weak (Fig. 4d), corresponding to a weaker control stationary wave (Fig. 4c). In most areas, the stationary wave change is to weaken the April climatological mean stationary waves in the control climate. The only exception is in the Southern Hemisphere (SH) extratropics, where the change in the stationary wave in Fig. 4d is in phase with the control in Fig. 4c. In July, the stationary wave changes (Fig. 4f) are confined mainly to the Tropics and the general tendency is again to weaken the climatological stationary waves in July (Fig. 4e). Notice, for example, the reduction in the strength of the Tibetan high. In October, the stationary wave changes due to climate change (Fig. 4g) resemble that of January, with a slight westward phase shift in the Tropics and much weaker centers in the NH extratropics. Examining the root mean square of the zonal variance as a function of latitude for all seasons at the 250-mb level (not shown) for the control and response, we notice a 30%–50% change in the amplitude of the tropical centers in January and July and of the Northern Hemispheric extratropical centers in January.

To quantify the degree of anticorrelation between the control integration's stationary wave and the response seen in Fig. 4, we show the spatial pattern correlation in the streamfunction between the response and the control, for each month and vertical level, for the whole globe (Fig. 5a), for the NH (Fig. 5b), and for the SH (Fig. 5c). The generally negative correlation confirms our previous impression of the weakening of the stationary wave field in response to climate change. The maximum negative correlation is found in the summer season in both hemispheres. For the NH winter, the negative correlation is partially compensated by the in-phase relationship between the stationary wave response pattern and the control simulation's pattern in the ex-

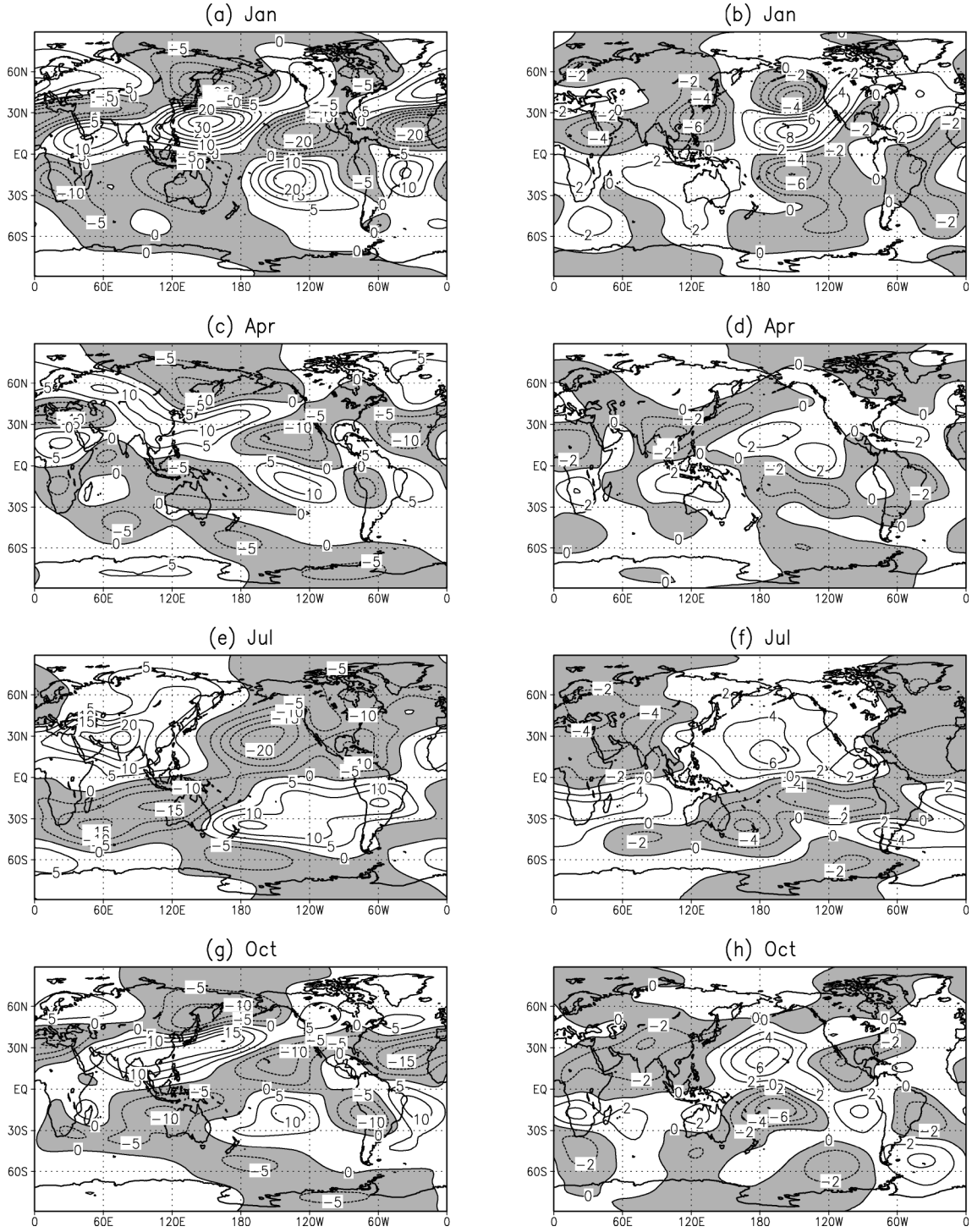

FIG. 4. Stationary wave streamfunction at 250 mb for (left) the control integration and (right) the climate change response, that is, the difference between the ensemble average climate change scenario integration and the control integration for (a), (b) Jan, (c), (d) Apr, (e), (f) Jul, and (g), (h) Oct. Contour intervals are 5×10^6 m^2 s^{-1} for control and 2×10^6 m^2 s^{-1} for the difference. Negative values are shaded.

tratropics. Positive correlations are found in the stratosphere (above approximately 150 mb); this aspect of the response does not merit further discussion since the model resolution is coarser there.

The reduction in stationary wave amplitude is further illustrated in Fig. 6, which shows the climate change response of the quantity shown in Fig. 2c, that is, the difference between the global integral of the square of

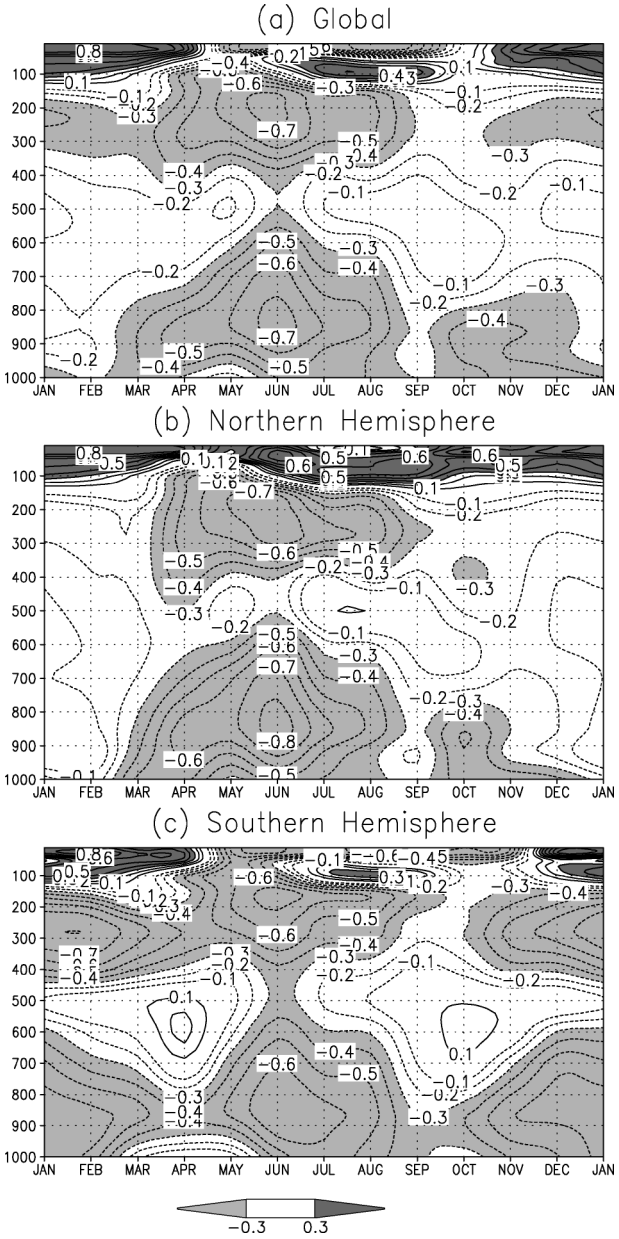

FIG. 5. Area-weighted spatial pattern correlation between the control integration's stationary wave streamfunction and the climate change response for (a) the whole globe, (b) the NH, and (c) the SH. Contour interval is 0.1, and correlations greater than 0.3 are heavily shaded and those less than −0.3 are lightly shaded.

the stationary wave streamfunction amplitude in the scenario and the control cases. The response of this measure of stationary wave amplitude is almost everywhere negative in the troposphere. Typical fractional reductions in global stationary wave streamfunction amplitude squared are 10%–15% and follow that of the seasonal cycle of the control integration.

The overall reduction in the lower-tropospheric stationary wave amplitude evident in Figs. 5 and 6 is shown in more detail in Fig. 7, which plots the streamfunction response at 850 mb for January and July along with the control-integration stationary wave field. We emphasize in addition the significant enhancement and eastward extension of the Aleutian low in NH winter (Fig. 7b). This indicates that, while the general tendency is a weakening of the stationary waves, the winter extratropical transients, which are known to maintain the Aleutian low (Held et al. 2002), may very well be intensified in the climate change scenario. This has been confirmed by examining the effect of the extratropical heating and transients.

In July, the low-level stationary wave response is, again, a weakening of the pattern. It is particularly noteworthy that the Asian monsoon circulation is weakened in the climate change scenario integrations, manifested by the anticyclone pair over the Asian monsoon region in Fig. 7d. The weakening of the monsoon circulation features related to climate change has also been noted in other climate change experiments (e.g., Meehl et al. 2000b).

The climate change response of the precipitation is illustrated in Fig. 8, along with the precipitation pattern of the control simulation. The gross features of the control simulation compare fairly well with observations (not shown), with three main centers of the intertropical convergence zone (ITCZ) associated with the equatorial landmass and the western Pacific warm pool in all months. The seasonal cycle of the meridional position of the ITCZ is also realistically represented. The Asian monsoon rainfall is well simulated, although there is excessive precipitation farther north near the foothills of the Tibetan Plateau and less rainfall over the west coast of India (Fig. 8e). The most notable feature of the precipitation response is the intense increase in precipitation in the tropical Pacific in the vicinity of the date line in all months. The precipitation is reduced in the South China Sea and the South Pacific convergence zone (SPCZ) region in January (Fig. 8b) and October (Fig. 8f). In April, the precipitation is reduced mainly over Southeast Asia. In July, the precipitation is clearly reduced in the Indian monsoon and enhanced farther north. Tropical precipitation is increased over Central and South America in all months. During boreal winter, we see that precipitation is increased over the Pacific storm track regions.

The increased precipitation over the central Pacific resembles that observed during an El Niño; thus, the accompanying response of the diabatic-heating forcing of the stationary waves is expected to be El Niño–like. [Notice that the maximum response is shifted farther to the west of the observed El Niño precipitation anomaly. This may be related to the fact that this model's ENSO precipitation anomalies also exhibit a westward-shifted bias (Knutson et al. 1999; Delworth et al. 2002).] Due to the dominance of the western Pacific heating center in the control, the central Pacific heating anomaly in the scenario case is indeed to reduce the zonally asymmetric component of the heating in the control. This qualita-

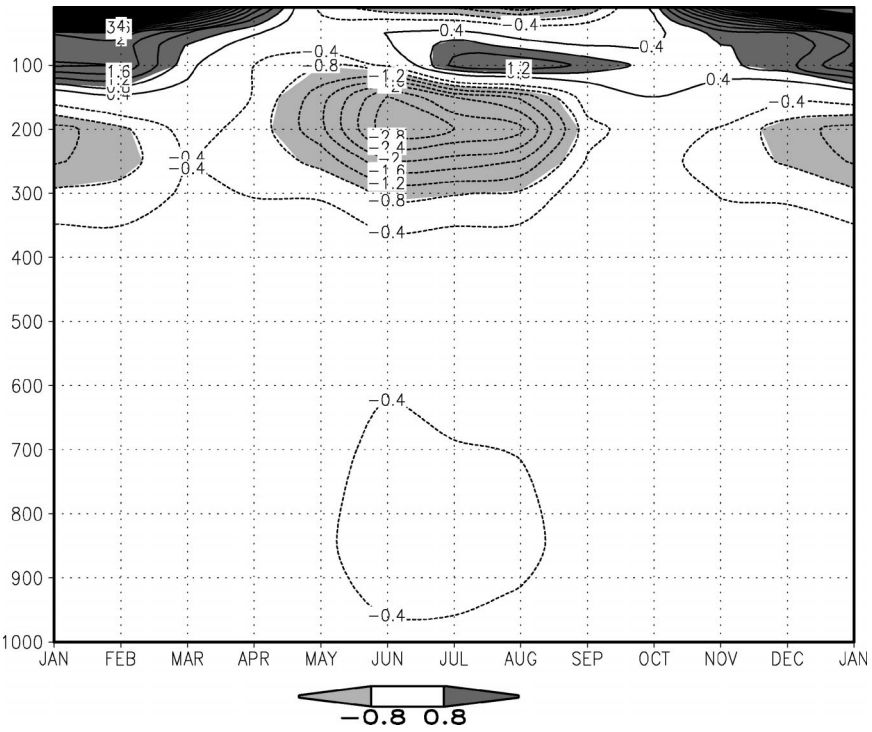

FIG. 6. Area-weighted global integral of the square of the stationary wave responses to climate change in streamfunction as a function of pressure and month. Contour interval is 0.4×10^{13} m^4 s^{-2}, and values greater than 0.8×10^{13} m^4 s^{-2} are heavily shaded and those less than -0.8×10^{13} m^4 s^{-2} are lightly shaded.

tively accounts for the general weakening of the stationary waves in the climate change scenario integrations. This type of El Niño–like pattern in precipitation has also been noticed in many climate change studies with increased CO_2 and sulfate aerosol concentrations (e.g., Knutson and Manabe 1998; Meehl et al. 2000, etc.).

4. Linear-model results

a. Decompositions of the response

We now use the linear steady-state model described in section 2b to analyze the forcing mechanisms of the stationary wave response. To evaluate the model's ability to reproduce the coupled model's stationary wave response, we solve (1) and (2) separately: We find the linear stationary wave solution, using as inputs the zonal mean basic state and the total forcing, that is, diabatic heating, orography, transients, and stationary nonlinearity, taken from the control (1) and the scenario ensemble (2). The difference between the scenario and control simulations gives $\delta\psi^*$, which is the linear model's representation of the coupled model's stationary wave response. The upper- and lower-tropospheric linear-model streamfunction response to the total forcing in January and July are shown in Fig. 9. The linear model reproduces the spatial pattern of the GCM response very well in both January and July. The amplitude, however, is slightly underestimated in the linear model, particularly for the low center over the Gulf of Alaska at both the upper and lower troposphere in January.

As described in section 2b, the linear model's stationary wave response $\delta\psi^*$ can be decomposed into parts associated with the climate change response in the basic state [$\delta\psi_b^*$ in (3) and (5)] and with the climate change response in the forcings [$\delta\psi_f^*$ in (3) and (4)]. This decomposition is shown for the upper-tropospheric streamfunction response in Fig. 10. Figures 10a and 10b show the effect of the basic-state change by calculating $\delta\psi_b^*$ for January and July. Figures 10c and 10d show the impact of the change of forcing by calculating $\delta\psi_f^*$ for the same months.[1]

Figure 10 shows that both parts of the decomposition in (3)–(5) contribute significantly to the total response and that, in many areas, the change in the zonal-mean basic state dominates over the change in the zonally asymmetric forcings. For example, Figs. 9a and 10a share many of the same features over the Pacific–North America region, as well as over Eurasia. In some re-

[1] In separate calculations (not shown), we have verified that the approximation in (4) is valid: it makes little difference whether the control or the perturbed mean state is used to calculate $\delta\psi_f^*$.

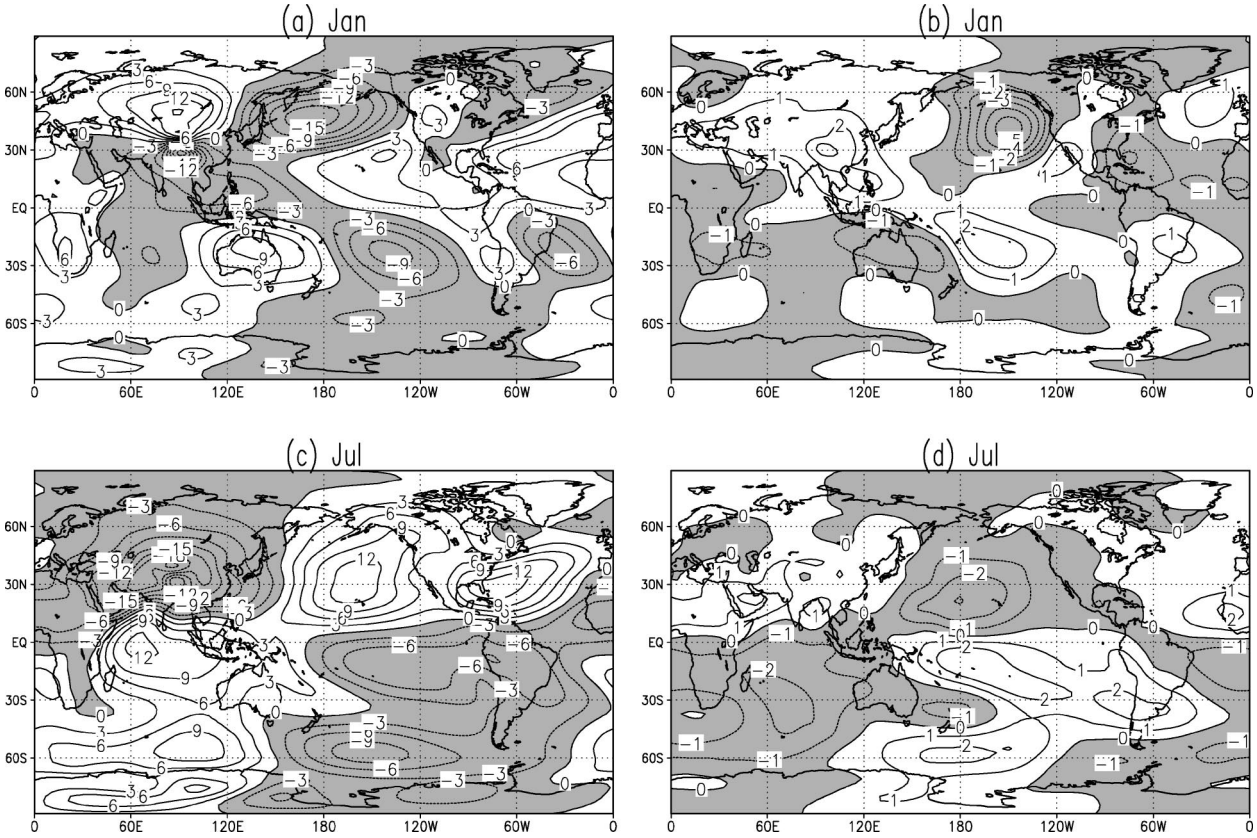

FIG. 7. Stationary wave streamfunction at 250 mb for (left) the control integration and (right) the climate change response for (a), (b) Jan, and (c), (d) Jul. Contour intervals are 3×10^6 m^2 s^{-1} for the control and 1×10^6 m^2 s^{-1} for the response. Negative values are shaded.

gions, for example, over eastern South America, the two parts shown in Figs. 10a and 10c reinforce each other, while in other regions, for example, over the northern Indian Ocean and Greenland, the two cancel. For the corresponding panels in July (Figs. 9b, 10b, and 10d), we see that much of the Western Hemisphere response is linked to the change in the basic state. Thus we conclude that the weakening of the stationary waves in the climate change scenario is also linked to the basic-state response throughout the year.

To better understand how the change in the basic state can drive a change in the stationary waves, we show, in Fig. 11, the coupled-model response of the zonal-mean zonal wind and the temperature for January and July. There is an increase in subtropical jet strength in both winter and summer hemispheres due to the tropical warming in the upper troposphere. The increase is stronger in the winter hemisphere in both months. The polar warming in the lower troposphere is accompanied by reduced westerlies at middle latitudes, most strongly in the NH winter. The upper-tropospheric wind changes are substantial in both hemispheres and seasons and can be expected to have a relatively large impact on the stationary wave responses to diabatic-heating forcing (Held and Ting 1990). The zonal-mean temperature reflects the tropospheric warming and stratospheric cooling in both months. The change in the thermal structure may also have an impact upon the stationary wave properties, but we have not yet investigated this issue in detail.

We next use the second decomposition, (6)–(8) in section 2b, to separate the contributions of the individual forcings to the response. As indicated in (7), this decomposition contains the effects of the change in basic state for the particular forcing and the effects of the change in the forcing itself. We decompose the January total response in Fig. 9a into that due to diabatic heating (Fig. 12a), transients (Fig. 12b), orography (Fig. 12c), and stationary nonlinearity (Fig. 12d). At first glance, none of the responses to any individual forcing resembles that in Fig. 9a very well, indicating that there is no single dominant forcing. Overall, the diabatic heating contribution is strongest and accounts for many of the stationary wave response features in the GCM (Fig. 7a) and in the linear model (Fig. 9a).

Notice that the diabatic-heating contribution in Fig. 12a is generally shifted westward of the response and that it has larger peak amplitude than the total pattern in Fig. 9a. The latter indicates that other contributions must interfere destructively with the diabatic heating contribution. In particular, we find that the contribution from the transient eddies, which is the second-strongest

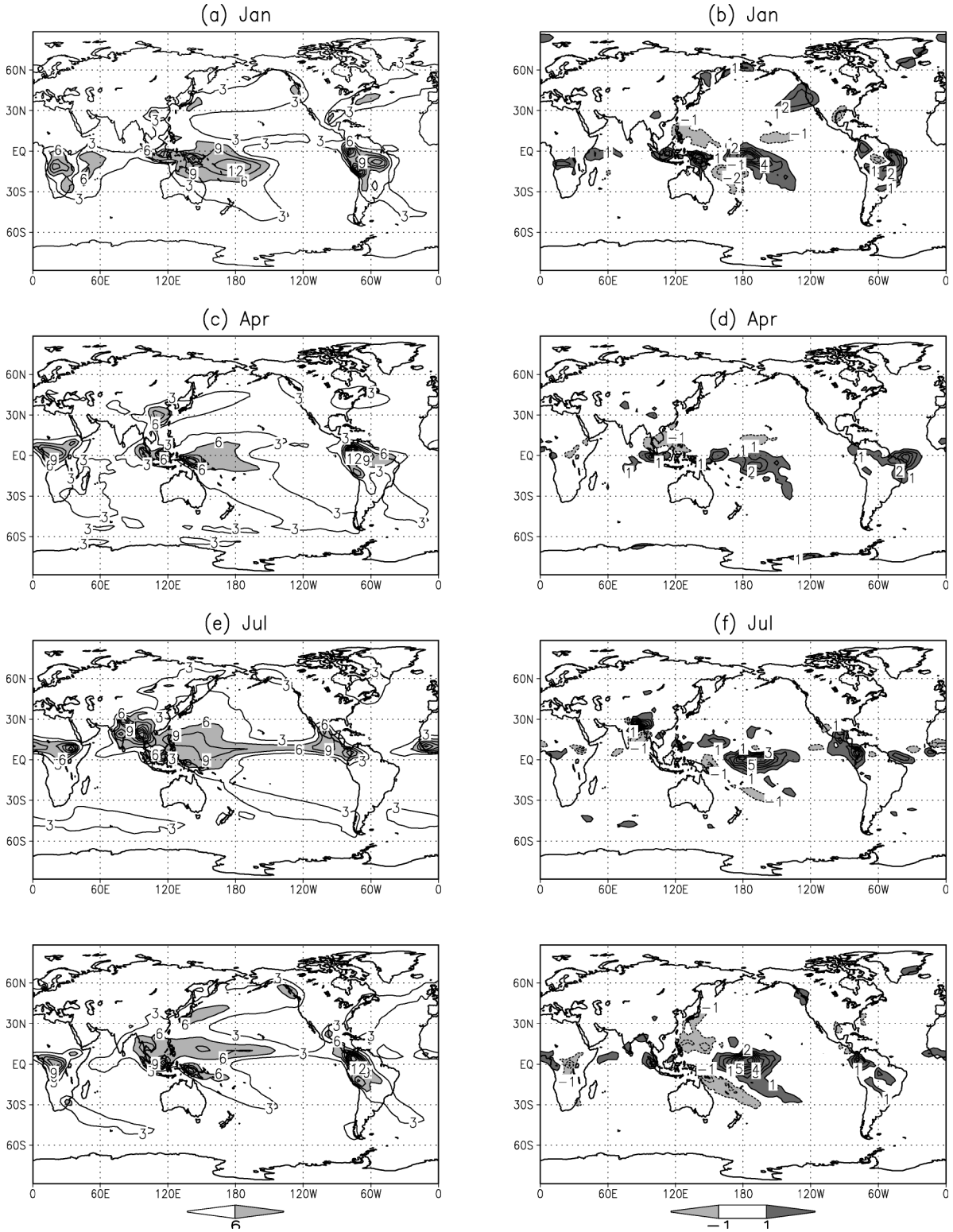

FIG. 8. Precipitation (mm day^{-1}) for (left) the control and (right) the climate change response for (a), (b) Jan, (c), (d) Apr, (e), (f) Jul, and (g), (h) Oct. Contour intervals are 3 mm day^{-1} for the control and 1 mm day^{-1} for the response.

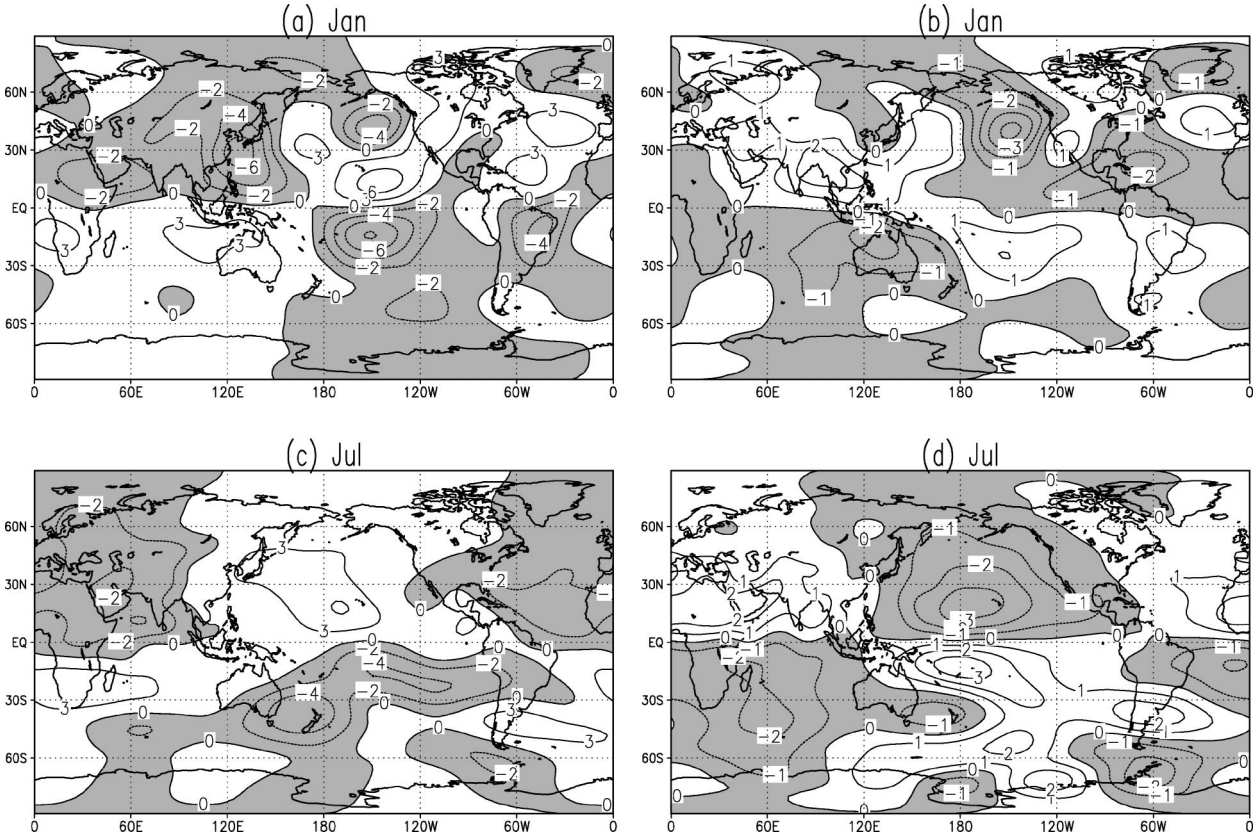

FIG. 9. Stationary wave streamfunction response of the linear model to climate change at (left) 250 and (right) 850 mb for (a), (b) Jan, and (c), (d) Jul. Contour interval is 2×10^6 m^2 s^{-1} for the upper level and 1×10^6 m^2 s^{-1} for the lower level. Negative values are shaded.

forcing effect, is moderately anticorrelated with the effect of heating (the spatial pattern correlation between Figs. 12a and 12b is -0.62); since their amplitudes are similar, this implies that there is a sizable cancellation between the two. The cancellation between the effect of heating and transients is more clearly seen when we examine the sum of the effect of heating and transients in Fig. 12e, which shows reduced peak amplitudes and roughly reproduces the main features in Fig. 9a. We repeated the decomposition shown in Fig. 12 but without the effect of the change in zonal-mean basic state: The cancellation between the effect of heating and transients is stronger in that case, confirming that the cancellation is due to the forcing itself, rather than the basic-state change.

The next-largest contributor to the total response is from the stationary nonlinearity (Fig. 12c). By adding this contribution to the heating and transient contributions (Fig. 12e), the pattern looks even more similar to Fig. 9a. Finally, the smallest contribution comes from the orography (Fig. 12c). The unimportance of this contribution is expected since it is largely controlled by changes in the lower-tropospheric zonal mean zonal flow between the control and the scenario cases, which are relatively small (Fig. 11a).

Given the large cancellation between the effect of heating and transients, we further separate these forcings into the tropical and extratropical parts. The results (not shown) indicate that the cancellation is mainly between the contributions from the heating and the transients in the Tropics; the extratropical contributions are relatively weak. Another decomposition of interest is to separate the transient eddy contributions from the vorticity, divergence, and thermal flux convergences. We find that the vorticity fluxes dominate (not shown), which is similar to the El Niño (Ting and Hoerling 1993; Hoerling and Ting 1994).

As for the January case, we use the second decomposition (6)–(8) to separate the forcing contributions to the July response. The main conclusions are similar: the effect of heating accounts for most of the features in the total response (Fig. 9c), with a westward phase shift; the shift of the pattern back toward the east is achieved by both the effect of transients and that of stationary nonlinearity (Figs. 13b,d–f); and the effect of orography is, once again, negligible.

Given the significant negative correlation between the linear model response to diabatic heating and that to transients, it is worthwhile to further explore the role of transients in January and July. In an idealized GCM

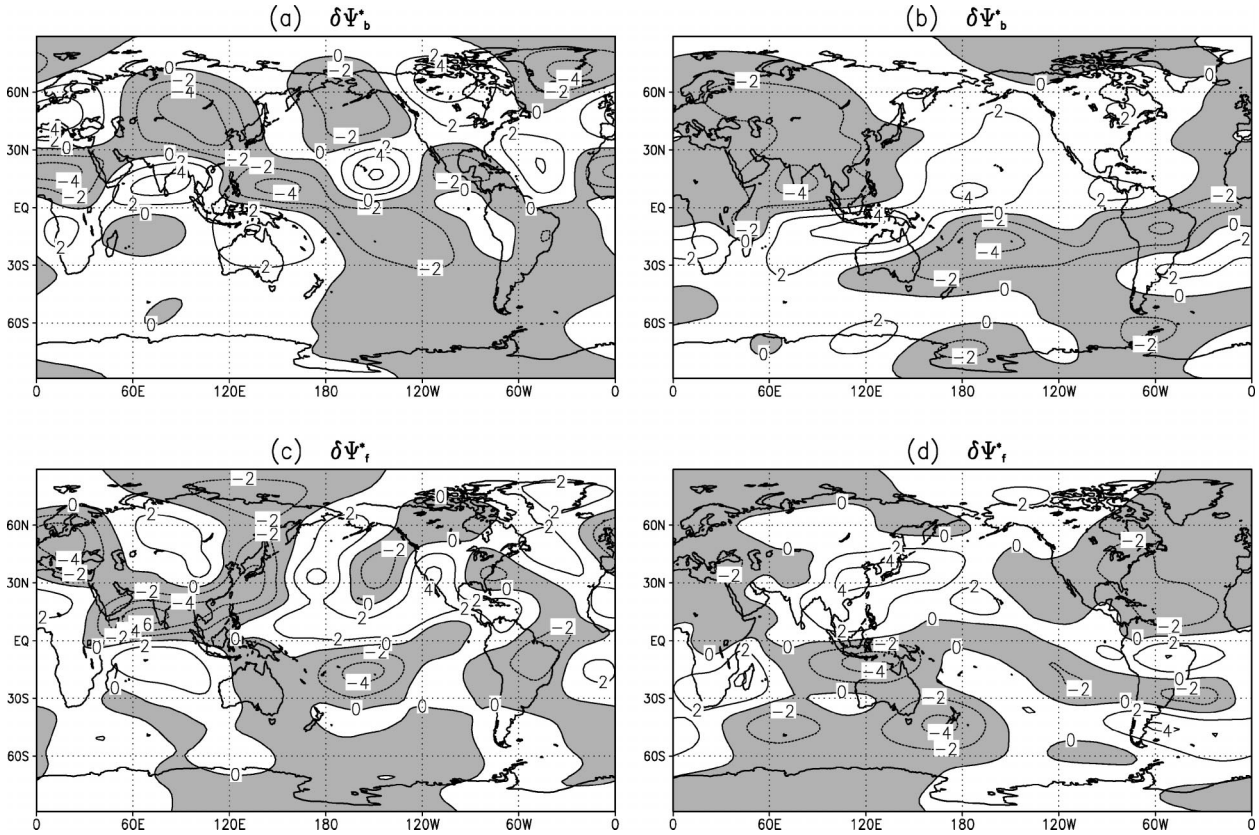

FIG. 10. Stationary wave 250-mb streamfunction response of the linear model to the climate-change-induced perturbation to the zonal-mean basic state for (a) Jan and (b) Jul, and stationary wave streamfunction response of the linear model to the climate-change-induced stationary wave forcings for (c) Jan and (d) Jul. Contour interval is 2×10^6 m^2 s^{-1} and negative values are shaded.

study with prescribed tropical sea surface temperature anomalies, Ting and Held (1990) find a similar cancellation between the effect of tropical heating and that of tropical transients in January and that the tropical vorticity transients can be mimicked by a simple 4-day damping in the Tropics. This is similarly done for the January and July responses, when the transient forcing is replaced by a 5-day damping in the vorticity equation between 30°S and 30°N and at the upper-tropospheric levels.

The linear model's 250-mb streamfunction response to a combination of diabatic heating and extratropical transients with a 5-day damping in the upper atmosphere, is shown in Fig. 14. The damping is included equatorward of 30° and at 0.17, 0.256, 0.354, 0.46, 0.569 σ levels, where the effects of tropical transients are the largest. The January and the July responses indicate that this response is equivalent to the response of the linear model subjected to the combined forcings of diabatic heating and transients in Figs. 12e and 13e. Thus, as in Ting and Held (1990), the role of the tropical transients in this case is acting as a simple damping to the effect of the diabatic heating.

b. *Relationship of climate change stationary wave response to El Niño*

Although the pattern of the Northern Hemisphere stationary wave climate change response bears some relationship to that of an El Niño, the linear-model analysis indicates important differences in the underlying dynamics between the two. First, the forcing mechanisms for the stationary wave response to climate change in January differ considerably from that of the current understanding of El Niño. As shown in Held et al. (1989), the extratropical response to El Niño is dominated by the effect of transients in the GFDL R15 model. Their results were further confirmed in observational data by Ting and Hoerling (1993) and Hoerling and Ting (1994). For the climate change response, however, the diabatic heating contribution is strongest and interferes destructively with the transients' contribution.

A second, more telling, difference is that the stationary wave response to the basic-state change is relatively large compared to the stationary wave response to the basic-state change in forcings (Fig. 10); that is, $|\delta\psi_b^*| > |\delta\psi_f^*|$ for the global warming response. But for the observed El Niño, the anomalous zonal-mean state is

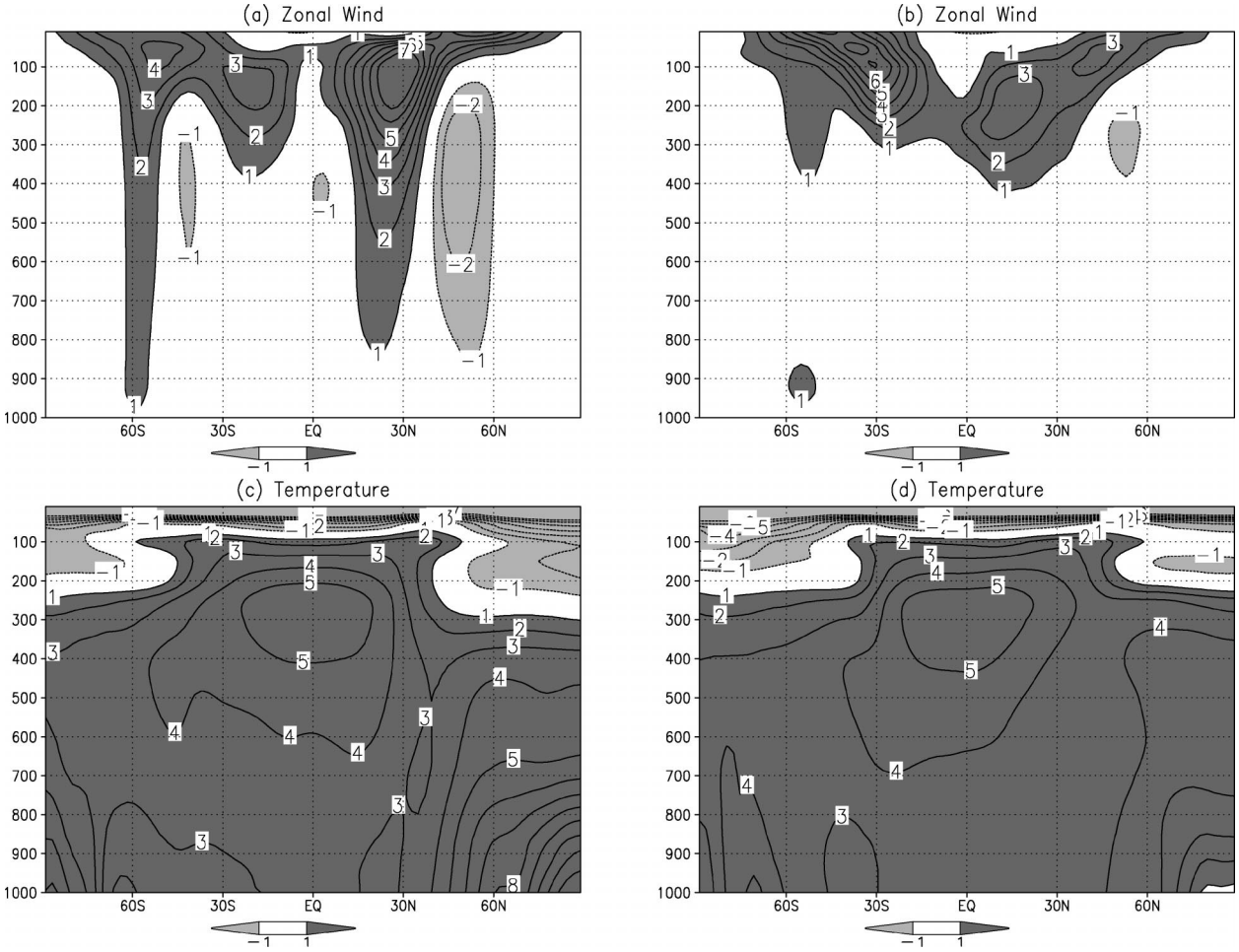

FIG. 11. (a), (b) Zonal-mean wind and (c), (d) temperature response to climate change for (a), (c) Jan and (b), (d) Jul. Contour interval is 1 m s^{-1} for wind and 1K for temperature, and values greater than 1 are heavily shaded and those less than −1 are lightly shaded.

found not to exert a significant effect on the stationary waves (Hoerling et al. 1995); that is, $|\delta\psi_b^*| < |\delta\psi_f|$ for the observed El Niño. Does this role reversal for $\delta\psi_b^*$ and $\delta\psi_f$ reflect an intrinsic difference in the way the model responds to tropical Pacific SST anomalies compared to the observations? The answer to this question appears to be ''no'': when we perform a linear stationary wave model analysis of warm versus cold tropical Pacific years of the model control simulation, we find that $|\delta\psi_b^*| < |\delta\psi_f^*|$, just as for the observed El Niño (figures not shown). [The fact that the model's tropical Pacific variability is of unrealistically low frequency and westward shifted compared to the observed (Delworth et al. 2002) is unimportant for this analysis.] The explanation is that the magnitude of the composite warm minus cold zonal-mean zonal wind anomalies is about half that of climate change response. Thus, the dynamics of the model and the observed response to tropical Pacific variability is similar, and this dynamics is quite different from the dynamics of the model response to global warming.

However, these conclusions stand at odds with the results of the R15 GFDL GCM's climate change response (Stephenson and Held 1993) discussed in the introduction. This lack of robustness may possibly be caused by the impact of increased atmospheric model resolution upon the simulation of the transient eddies. It may also reflect the inclusion of sulfate aerosols in the current climate change scenario. Another possibility is the strong precipitation response in the central Pacific, which seems to be a feature that is unique to this model (A. J. Broccoli 2002, personal communication). Whether the El Niño–like responses seen in other climate change experiments also have forcing mechanisms that are distinct from those of the El Niño itself is worth further study.

5. Summary and conclusions

The stationary wave response to the IS92a global warming scenario is very robust in the GFDL R30 GCM. For all months, the response consists of a weak-

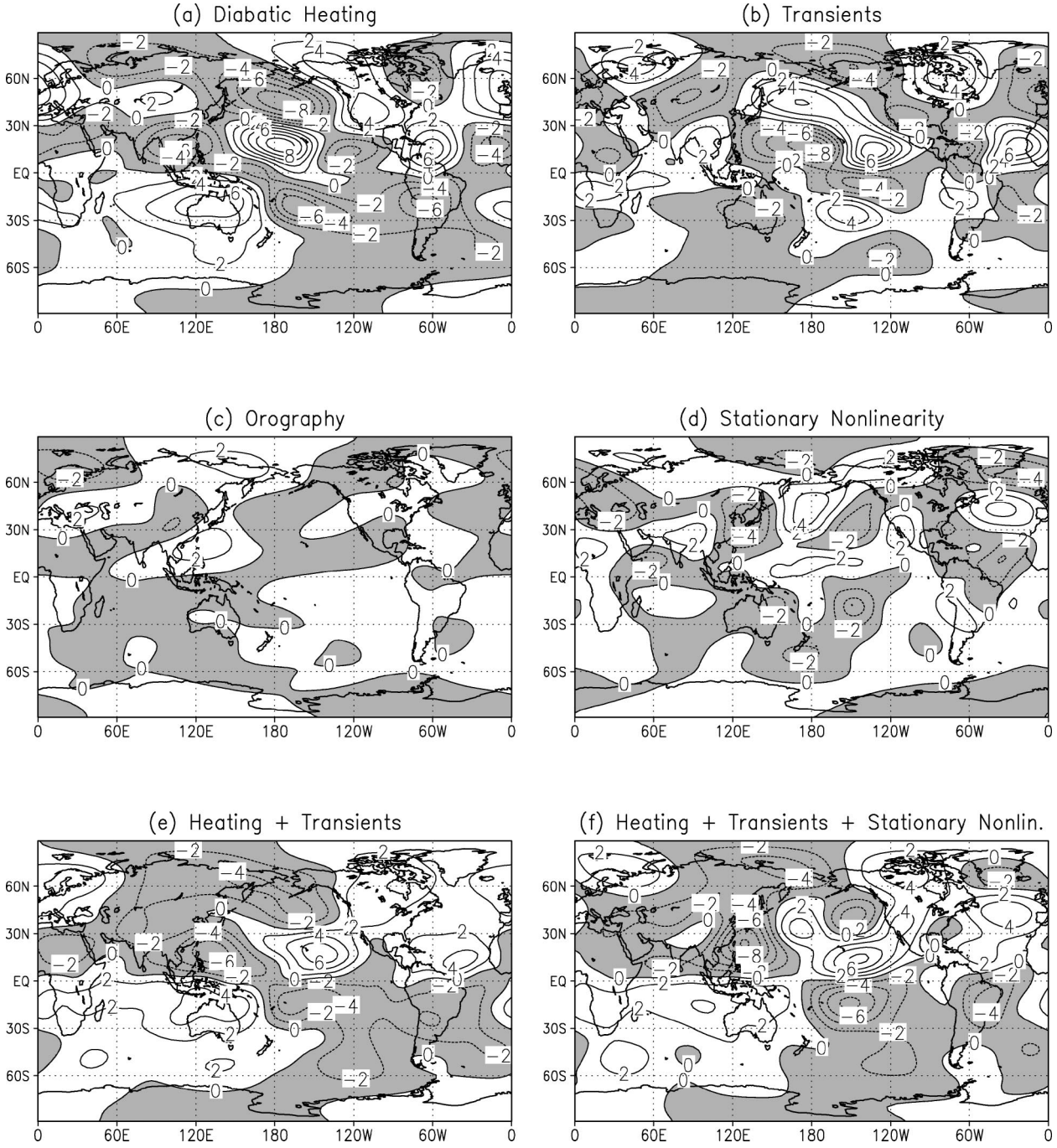

FIG. 12. Linear model 250-mb stationary wave response, in Jan, to forcings from (a) diabatic heating; (b) transients; (c) orography; (d) stationary nonlinearity; (e) the sum of diabatic heating and transient forcing; and (f) the sum of diabatic heating, transients, and stationary nonlinearity. Contour interval is 2×10^6 m^2 s^{-1}. Negative values are shaded.

ening of the tropospheric stationary waves. This weakening effect in the troposphere is particularly strong in the summer season. The monsoon circulation as seen in the stationary wave fields, in particular of the East Asian monsoon, is thus suppressed in the climate change scenario, a conclusion similar to other climate change studies when sulfate aerosols are included (e.g., Meehl et al. 2000b; Mitchell and Johns 1997). In NH winter, the changes in the stationary wave pattern resemble an El Niño response (see Fig. 4 in Hoerling and Ting 1994) with anticyclone pairs in the eastern subtropical Pacific and a cyclone pair over the subtropical western Pacific. A deep low over the Aleutian region in the upper troposphere is also noted. The deep low over the Aleutian

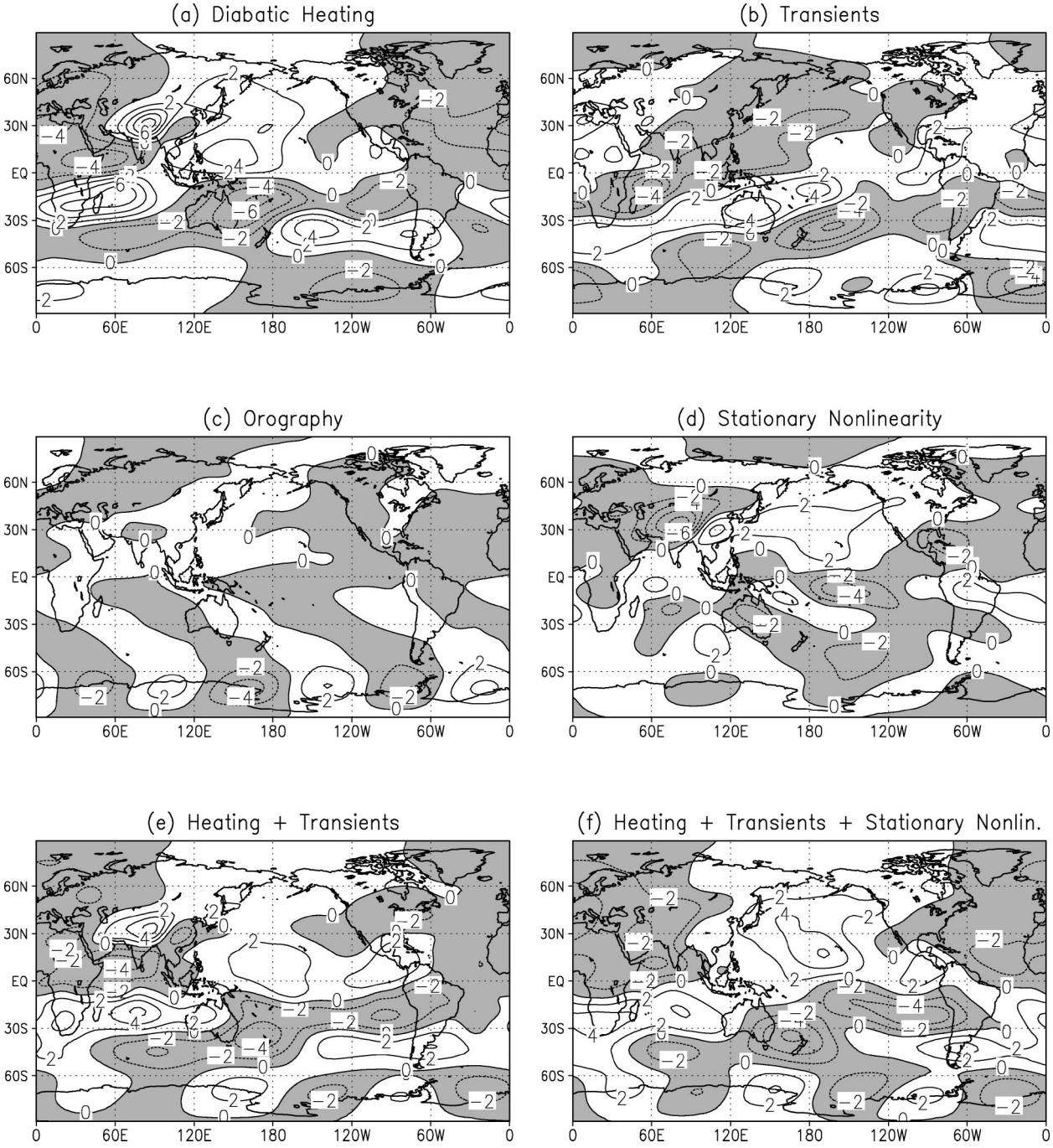

FIG. 13. As in Fig. 12 but for Jul.

region and the anticyclone over the eastern subtropical Pacific induces an eastward extended subtropical jet, which brings more precipitation to the west coast of the United States (Fig. 5).

Possible causes for the stationary wave change during a warming environment include changes in the zonal mean flow, changes in the heating structure, and changes in transient eddy behavior due to the shift in jet stream. The linear model reproduces the coupled model's stationary wave response remarkably well when all the effects of all the forcings are included. The linear decompositions of the response show that the mechanisms of response are quite unlike El Niño, being dominated by the change to the zonal-mean circulation and the diabatic heating forcing both in January and July. The reduction in the amplitude of the stationary waves in the climate change scenario is primarily caused because of the change in the zonal-mean basic state. The effects

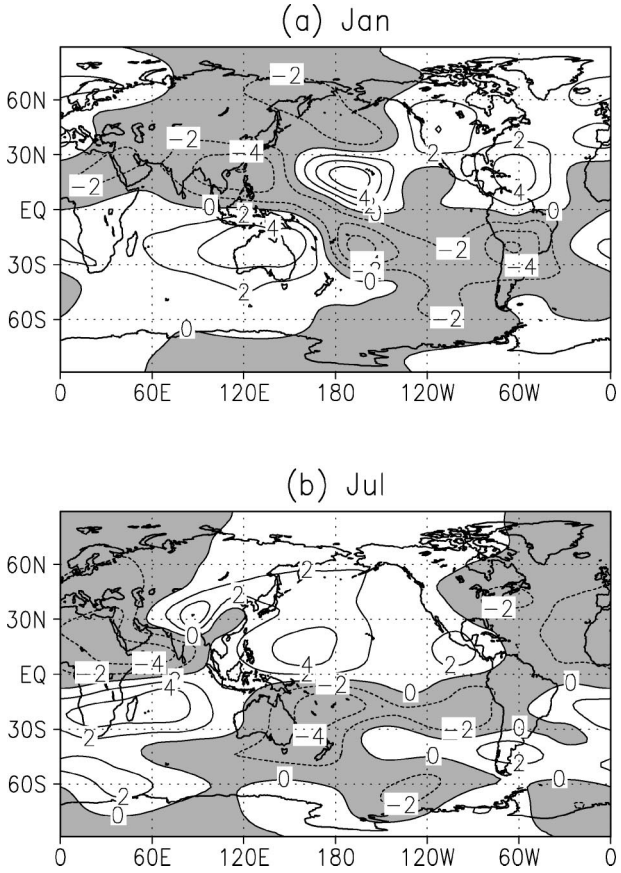

FIG. 14. Linear model response in (a) Jan and (b) Jul to diabatic heating and extratropical transients with the effect of tropical transients parameterized as a 5-day damping at 0.17, 0.256, 0.354, 0.46, 0.569 σ levels.

of the diabatic heating also contribute to the reduction of amplitude.

The conclusion that the change to the zonal-mean basic state is an important driver of the stationary wave response in the model is of great interest. It points out a potential pitfall in the linear stationary wave modeling theory in which the basic state and the forcings are assumed to be independent. On the other hand, this conclusion provides a potentially useful starting point for further analysis of the extratropical circulation response to global warming. Several models demonstrate similar circulation responses to global warming in both hemispheres, including an increase in upper-tropospheric winds and positive annular mode trends (Shindell et al. 1999, 2001; Fyfe et al. 1999; Gillet et al. 2002); we note that no positive Northern Annular Mode trend is seen in the GFDL R30 model (Kushner et al. 2001). Understanding the robust aspects of the zonal-mean response to warming could be simpler than, or at least be independent from, understanding the change to the zonally asymmetric forcings. Following the philosophy outlined in Held et al. 2003 (stationary wave review) we could thus consider a three-step procedure toward developing a theory of the circulation response to global warming to 1) explain the zonally symmetric component of the change, 2) use stationary wave models to explain the zonally asymmetric component, and 3) understand the leading order interactions of the two responses.

Acknowledgments. We are grateful to Drs. Isaac Held and Gabriel Lau and two anonymous reviewers for comments and suggestions that have helped improve the presentation of the paper. This research was supported by the National Science Foundation Grant ATM 00-00585.

REFERENCES

Branstator, G., 1992: The maintenance of low-frequency atmospheric anomalies. *J. Atmos. Sci.*, **49,** 1924–1945.

Cai, W., and P. H. Whetton, 2001: A time-varying greenhouse warming pattern and the tropical–extratropical circulation linkage in the Pacific Ocean. *J. Climate*, **14,** 3337–3355.

Chen, S. C., and K. E. Trenberth, 1988a: Forced planetary waves in the Northern Hemisphere winter: Wave-coupled orographic and thermal forcings. *J. Atmos. Sci.*, **45,** 657–680.

——, and ——, 1988b: Orographically forced planetary waves in the Northern Hemisphere: Steady state model with wave-coupled lower boundary formulation. *J. Atmos. Sci.*, **45,** 657–681.

Delworth, T. L., R. J. Stouffer, K. W. Dixon, M. J. Spelman, T. R. Knutson, A. J. Broccoli, P. J. Kushner, and R. T. Wetherald, 2002: Review of simulations of climate variability and change with the GFDL R30 coupled climate model. *Climate Dyn.*, **19,** 555–574.

Fyfe, J. C., G. J. Boer, and G. M. Flato, 1999: The Arctic and Antarctic Oscillations and their projected changes under global warming. *Geophys. Res. Lett.*, **26,** 1601–1604.

Gillett, N. P., M. R. Allen, and K. D. Williams, 2002: The role of stratospheric resolution in simulating the Arctic Oscillation response to greenhouse gases. *Geophys. Res. Lett.*, **29,** 1381–1384.

Goswami, B. N., 1998: Interannual variations of Indian summer monsoon in a GCM: External conditions versus internal feedbacks. *J. Climate*, **11,** 501–522.

Haywood, J., R. Stoffer, R. Wetherald, S. Manabe, and V. Ramaswamy, 1997: Transient response of a coupled model to estimated changes in greenhouse gas and sulphate concentrations. *Geophys. Res. Lett.*, **24,** 1335–1338.

Held, I. M., and M. Ting, 1990: Orographic versus thermal forcing of stationary waves: The importance of the mean low-level wind. *J. Atmos. Sci.*, **47,** 495–500.

——, S. W. Lyons, and S. Nigam, 1989: Transients and extratropical response to the El Niño. *J. Atmos. Sci.*, **46,** 163–174.

——, M. Ting, and H. Wang, 2002: Northern winter stationary waves: Theory and modeling. *J. Climate*, **15,** 2125–2144.

Hoerling, M. P., and M. Ting, 1994: Organization of extratropical transients during El Niño. *J. Climate*, **7,** 745–766.

——, ——, and A. Kumar, 1995: Zonal flow–stationary wave relationship during El Niño: Implications for seasonal forecasting. *J. Climate*, **8,** 1838–1852.

Knutson, T. R., and S. Manabe, 1995: Time-mean response over the tropical Pacific to increased CO_2 in a coupled ocean–atmosphere model. *J. Climate*, **8,** 2181–2199.

——, and ——, 1998: Model assessment of decadal variability and trends in the tropical Pacific Ocean. *J. Climate*, **11,** 2273–2296.

——, T. L. Delowrth, K. W. Dixon, and R. J. Stouffer, 1999: Model assessment of regional surface temperature trends (1949–1997). *J. Geophys. Res.*, **104,** 30 981–30 996.

Kushner, P. J., I. M. Held, and T. L. Delworth, 2001: Southern Hemisphere atmospheric circulation response to global warming. *J. Climate*, **14,** 2238–2249.

Liu, A. Z., M. Ting, and H. Wang, 1998: Maintenance of circulation anomalies during the 1988 drought and 1993 floods over the United States. *J. Atmos. Sci.,* **55,** 2810–2832.

Meehl, G. A., and W. M. Washington, 1996: El Niño-like climate change in a model with increased atmospheric CO_2 concentrations. *Nature,* **382,** 56–60.

——, W. D. Collins, B. A. Boville, J. T. Kiehl, T. M. Wigley, and J. M. Arblaster, 2000a: Response of the NCAR Climate System Model to increased CO_2 and the role of physical processes. *J. Climate,* **13,** 1879–1898.

——, W. M. Washington, J. M. Arblaster, T. W. Bettgo, and W. G. Strand Jr., 2000b: Anthropogenic forcing and decadal climate variability in sensitivity experiments of twentieth- and twenty-first-century climate. *J. Climate,* **13,** 3728–3744.

Mitchell, J. F. B., and T. C. Johns, 1997: On the modification of global warming by sulphate aerosols. *J. Climate,* **10,** 245–267.

——, ——, J. Gregory, and S. Tett, 1995: Climate response to increasing levels of greenhouse gases and sulphate aerosols. *Nature,* **376,** 501–504.

Nigam, S., I. M. Held, and S. W. Lyons, 1986: Linear simulation of the stationary eddies in a general circulation model. Part I: The no-mountain model. *J. Atmos. Sci.,* **43,** 2944–2961.

——, ——, and ——, 1988: Linear simulation of the stationary eddies in a GCM. Part II: The ''mountain'' model. *J. Atmos. Sci.,* **45,** 1433–1452.

Shindell, D. T., R. L. Miller, G. Schmidt, and L. Pandolfo, 1999: Simulation of recent northern winter climate trends by greenhouse gas forcing. *Nature,* **399,** 452–455.

——, G. A. Schmidt, R. L. Miller, and D. Rind, 2001: Northern Hemisphere winter climate response to greenhouse gas, ozone, solar, and volcanic forcing. *J. Geophys. Res.,* **106,** 7193–7210.

Stephensen, D. B., and I. M. Held, 1993: GCM response of northern winter stationary waves and storm tracks to increasing amounts of carbon dioxide. *J. Climate,* **6,** 1859–1870.

Ting, M., 1994: Maintenance of northern summer stationary waves in a GCM. *J. Atmos. Sci.,* **51,** 3286–3308.

——, and I. M. Held, 1990: The stationary wave response to a tropical SST anomaly in an idealized GCM. *J. Atmos. Sci.,* **47,** 2546–2566.

——, and M. P. Hoerling, 1993: The dynamics of stationary wave anomalies during the 1986/87 El Niño. *Climate Dyn.,* **9,** 147–164.

——, and N.-C. Lau, 1993: A diagnostic and modeling study of the monthly mean wintertime anomalies appearing in a 100-year GCM experiment. *J. Atmos. Sci.,* **50,** 2845–2867.

——, M. P. Hoerling, T. Xu, and A. Kumar, 1996: Northern Hemisphere teleconnection patterns during extreme phases of the zonal mean circulation. *J. Climate,* **9,** 2614–2633.

——, H. Wang, and L. Yu, 2001: Nonlinear stationary wave maintenance and seasonal cycle in the GFDL R30 GCM. *J. Atmos. Sci.,* **58,** 2331–2354.

Valdes, P. J., and B. J. Hoskins, 1989: Linear stationary wave simulations of the time-mean climatological flow. *J. Atmos. Sci.,* **46,** 2509–2527.

Wang, H., and M. Ting, 1999: Seasonal cycle of the climatological stationary waves in the NCEP–NCAR reanalysis. *J. Atmos. Sci.,* **56,** 3892–3919.